Clim. Past Discuss., 9, 6605–6633, 2013
www.clim-past-discuss.net/9/6605/2013/
doi:10.5194/cpd-9-6605-2013
© Author(s) 2013. CC Attribution 3.0 License.

Climate of the Past Discussions
Open Access

This discussion paper is/has been under review for the journal Climate of the Past (CP).
Please refer to the corresponding final paper in CP if available.

Impact of geomagnetic events on atmospheric chemistry and dynamics

I. Suter[1], R. Zech[2], J. G. Anet[1], and T. Peter[1]

[1]Institute for Atmospheric and Climate Science ETH, Zürich, Switzerland
[2]Geological Institute ETH, Zürich, Switzerland

Received: 21 October 2013 – Accepted: 25 November 2013 – Published: 17 December 2013

Correspondence to: I. Suter (suter.ivo@bluewin.ch)

Published by Copernicus Publications on behalf of the European Geosciences Union.

Abstract

Geomagnetic events, i.e. short periods in time with much weaker geomagnetic fields and substantial changes in the position of the geomagnetic pole, occurred repeatedly in the Earth's history, e.g. the Laschamp Event about 41 kyr ago. Although the next such event is certain to come, little is known about the timing and possible consequences for the state of the atmosphere and the ecosystems. Here we use the global chemistry climate model SOCOL-MPIOM to simulate the effects of geomagnetic events on atmospheric ionization, chemistry and dynamics. Our simulations show significantly increased concentrations of nitrogen oxides (NO_x) in the entire stratosphere, especially over Antarctica (+15 %), due to enhanced ionization. Hydrogen oxides (HO_x) are also produced in greater amounts (up to +40 %) in the tropical and subtropical lower stratosphere, while their destruction by reactions with enhanced NO_x prevails over the poles and in high altitudes (by −5 %). Stratospheric ozone concentrations decrease globally above 20 km by 1–2 % and at the northern hemispheric tropopause by up to 5 % owing to the accelerated NO_x-induced destruction. A 5 % increase is found in the southern lower stratosphere and troposphere. In response to these changes in ozone and the concomitant changes in atmospheric heating rates, the Arctic vortex intensifies in boreal winter, while the Antarctic vortex weakens in austral winter and spring. Surface wind anomalies show significant intensification of the southern westerlies at their poleward edge during austral winter and a pronounced northward shift in spring. This is analogous to today's poleward shift of the westerlies due to the ozone hole. It is challenging to robustly infer precipitation changes from the wind anomalies, and it remains unclear, whether the Laschamp Event could have caused the observed glacial maxima in the southern Central Andes. Moreover, a large impact on the global climate seems unlikely.

1 Introduction

Galactic Cosmic Rays (GCRs) are highly energetic particles (1 MeV–5×10^{13} MeV) from outside the heliosphere, mainly composed of protons and α-particles, which continuously impinge on the atmosphere (Bazilevskaya et al., 2008). The Earth is shielded against the incoming particles, first by the solar magnetic field and the solar wind, which deflect GCRs away from the Earth leading to a decrease in GCR penetration into the inner heliosphere, particularly during phases of increased solar activity (Potgieter, 1998), second, at distances of only a few Earth radii, by the geomagnetic field, at least at lower latitudes. However, neither the geomagnetic field nor the solar activity are constant over time. During the so-called Laschamp Event ~ 41 thousand years ago (kyr), for example, the geomagnetic field experienced a full reversal, i.e. the direction of the geomagnetic polarity reversed completely, and the field strength decreased to only ~ 10 % for several hundred years. After the excursion the field rapidly recovered strength and returned to normal polarity (Nowaczyk et al., 2012). Possible effects for the atmosphere and the ecosystems have not attracted much scientific attention so far, although it is foreseeable that geomagnetic events will also occur in the future. The motivation for this study stems from the finding that glaciers in the relatively arid southern Central Andes at ~ 30–40° S reached their maximum extents at ~ 40 kyr, long before the global last glacial maximum at ~ 20 kyr (Lowell et al., 1995; Denton et al., 1999; Espizua, 2004; Zech et al., 2007, 2008, 2011). As glaciers are not only sensitive to temperature changes, but also to precipitation (and particularly so under arid conditions), this has been interpreted as indicating a northward shift of the southern hemispheric westerly winds (SWW) and increased precipitation at ~ 40 kyr. A possible link to the Laschamp Event has been suggested (Zech et al., 2011), which has its reasoning in the fact that GCRs have a significant influence on the upper tropospheric and stratospheric chemistry through ionization and the production of NO_x and HO_x, which can lead to catalytic destruction of stratospheric ozone and production of tropospheric ozone (Calisto et al., 2011). A massive ozone hole during the Laschamp

Event has in fact recently been suggested as potential factor favouring the extinction of the Neanderthal (Valet and Valladas, 2010). Moreover, the ozone changes affect atmospheric heating rates, which in turn can result in altered temperature gradients and changing wind patterns (Sinnhuber et al., 2012). Already Thompson and Solomon (2002) suggested that stratospheric ozone depletion can cause the southern hemispheric (SH) jet to shift. The exact processes and mechanisms, however, are poorly understood. The observed southward shift of the SWW over the last few decades, for example, was driven at least partly by stratospheric ozone depletion (Cai and Cowan, 2007; Son et al., 2008). Shifting SWW due to GCRs or other forcings may have had and potentially will have a global effect on climate, because they drive Southern Ocean upwelling and deep ocean ventilation, i.e. the release of carbon dioxide from the deep ocean (Toggweiler et al., 2006). Links between changes in the geomagnetic field and global climate in the geologic past have indeed been made (Christl et al., 2004), but all mechanisms involved in getting from enhanced GCRs to a change in global climate need to be investigated in much more detail, before they can be taken more seriously into consideration.

Up to now, to the best of our knowledge, no chemistry-climate modelling study of the Laschamp event has been done. This study thus investigates the possible influence of geomagnetic events and solar modulation on the GCR-induced ionization in the atmosphere, atmospheric chemistry and dynamics using the atmosphere-ocean-chemistry climate model SOCOL-MPIOM. We carried out seven 51 yr long simulations, which differed in strength of the geomagnetic dipole moment (M), the latitude of the geomagnetic pole and the solar modulation potential (ϕ).

2 Model description

The model SOCOL-MPIOM consists of the middle atmosphere version of the global circulation model ECHAM5 (Roeckner et al., 2003, 2006; Manzini et al., 2006), a modified version of the chemistry model MEZON (Rozanov et al., 1999, 2001; Egorova et al.,

2003; Hoyle, 2005) and has been coupled with OASIS3 (Valcke, 2013) to the ocean model MPI-OM (Marsland et al., 2003). Version 1 and 2 of SOCOL, based on MA-ECHAM4, have been validated by Egorova et al. (2005) and Schraner et al. (2008). SOCOLv3 was recently developed by Stenke et al. (2013), who coupled the chemistry and dynamics routines to MA-ECHAM 5.4.00, improved the advection scheme for chemical species and enabled it to be fully parallelized. SOCOLv3 improves some previous deficiencies in chemical transport. The chemical processes triggered by solar energetic particles (SEP) and GCRs have recently been implemented in SOCOLv2 by Calisto et al. (2011) and in SOCOLv3 by Anet et al. (2013).

The CRAC:CRII (Cosmic Ray Atmospheric Cascade: Application for Cosmic Ray Induced Ionization, Usoskin and Kovaltsov, 2006; Usoskin et al., 2010) model was used to describe the effect of GCRs in the entire horizontal and vertical model domain. CRAC:CRII is able to calculate the effect of ϕ and the geomagnetic field on GCRs. The solar modulation potential ϕ is used to describe the deceleration of precipitating particles due to their interaction with the solar wind (Gleeson and Axford, 1968; Caballero-Lopez and Moraal, 2004; Usoskin et al., 2005). It influences the amount and energy spectrum of particles which pass the heliosphere and reach Earth's magnetopause. The geomagnetic field M affects the further penetration into the Earth's atmosphere depending on the incoming energy spectrum and latitude. CRAC:CRII performed a Monte-Carlo simulation of the ionization cascade following the penetration of an energetic particle into the atmosphere. The ionization is a function of altitude, geomagnetic latitude, field strength and the solar activity. The ionization rates calculated by CRAC:CRII are tabulated and converted to a NO_x and HO_x production rate, by means of simple parameterization, since SOCOL does not treat ion-chemistry explicitly. The conversion factor for NO_x is 1.25 nitrogen atoms per ion pair (Porter et al., 1976). 45 % of which yield N(^{4}S) and 55 % yield N(^{2}D). The latter instantaneously converts into NO via N(^{2}D) + O_2 → NO + O. For HO_x we implemented the parameterization by Solomon et al. (1981). They examined the thermodynamics of ion and neutral chemistry during charged particle precipitation events to describe odd hydrogen production

depending on altitude and ionization rate and found values between 1.9 and 2 odd hydrogen molecules produced per ion pair below 60 km altitude.

We use SOCOL-MPIOM in T31 horizontal resolution, i.e. with an approximate grid spacing of 3.75° × 3.75° and 39 vertical hybrid sigma-p levels, spanning the atmosphere from surface to 1 Pa (~ 80 km). It contains 41 chemical species, which interact via 140 gas phase, 46 photolytic and 16 heterogeneous reactions.

MPI-OM is based on the primitive equations and uses hydrostatic and Boussinesq approximations. Horizontal discretization is on an orthogonal curvilinear C-grid, while in the vertical isopycnic coordinates are used. MPI-OM includes a dynamic and thermodynamic sea ice model.

3 Model setup

A 400 yr spin-up run of the model was performed under glacial conditions at ~ 41 kyr. The Earth's orbital parameters were set accordingly. The initial land surface data set (e.g. ice cover) and ocean temperatures are from an earlier glacial simulation with ECHAM5 (M. Thürkow, personal communication, 2012). The atmosphere was in a pristine state, we set concentrations of greenhouse gases and ozone depleting substances to pre-industrial values ([CH_4], [N_2O], [CO_2] from Schilt et al., 2010, [CH_3Cl] from Saltzman et al., 2009, [CH_3Br] from Liebowitz et al., 2009). After spin-up the model has a globally averaged mean annual 2 m temperature of ~ 284.25 K. This is about 4 K colder than present day conditions and in reasonable agreement with paleo-records for the last glacial maximum and other model results (Mix et al., 2001; Braconnot et al., 2007; Jansen et al., 2007).

We then branched off seven 51 yr long simulations (Table 1). While trace gas concentrations, intensity of the geomagnetic field, position of the geomagnetic pole and solar properties were further held constant for the reference run, three simulations were carried out with only 10 % of the dipole moment (M10), i.e. with significantly reduced field strength. In two of these three simulations the position of the pole was

varied additionally, once to 45° and once to 0° (M10P45 and M10P0), in order to perform runs under conditions close to the Laschamp Event. Three more simulations were carried out as sensitivity tests. M0 has a dipole moment set to zero. PHI0 has a normal magnetic field, but solar modulation potential set to zero. M0PHI0 has both, dipole moment and the solar modulation potential ϕ, set to zero. (Note that we simplified the geomagnetic field as a dipole in all simulations without higher order geomagnetic field components.)

4 Results and discussion

4.1 Changes in atmospheric chemistry

4.1.1 NO_x concentrations

The zonally averaged mean annual NO_x concentrations ($[NO_x] = [NO] + [NO_2]$) show significant increases in the stratosphere in all 6 simulations (Fig. 1). Simulations M10, M10P45, M10P0 and M0 look very similar, since they all have a weak geomagnetic field, which allows more cosmic radiation to reach the atmosphere and results in enhanced ionization and production of N, NO and OH. A change of the position of the geomagnetic pole has a smaller additional effect. The greatest effects of enhanced ionization occur between 16–25 km, the Pfotzer Maximum (Bazilevskaya and Svirzhevskaya, 1998). NO_x shows a significant increase in the entire stratosphere above 200 hPa (~ 12 km). Antarctic stratospheric concentrations rise by 15 %. The Arctic shows a smaller increase of 5 %. This asymmetry between the northern and Southern Hemisphere is due to the fact that reference NO_x concentrations around 100 hPa are lower in the Southern Hemisphere. No strong increase can be found in the troposphere, some regions even show a small decrease, although without statistical significance on the 5 % confidence level. Note that although the strength of the magnetic field strongly controls the GCR intensity at low latitudes (due to the perpendicular

orientation of the field), the long lifetime of NO_x allows for an efficient latitudinal distribution. In PHI0 NO_x concentrations increase particularly at high latitudes, because the magnetic field lines on the poles are almost parallel to the incoming GCRs. These are therefore mainly modulated by ϕ, while the magnetic field has a minor influence. Vice versa, the effect of ϕ is small at low latitudes since there the magnetic field provides efficient shielding (as long as the field intensities are not reduced). The M0PHI0 simulation represents the most extreme case of enhanced ionization in our study. The absence of the geomagnetic field and of the solar modulation potential ϕ, i.e. no shielding from GCRs, causes a NO_x increase of more than 20 % in the lower stratosphere.

4.1.2 HO_x concentrations

Concentrations of hydrogen oxides ($[HO_x]=[HO_2] + [OH] + [H]$), which are also produced by galactic cosmic rays, reveal a very similar pattern for the experiments M10, M10P45, M10P0 and M0, indicating again that the pole position is less important for changes in ionization than field strength (Fig. 2). Distinct increases in HO_x (+50 %) are found in the tropical and subtropical upper troposphere and lower stratosphere (UTLS) up to 25 km. The strong increase emphasises the importance of GCRs as a HO_x source in those altitudes. HO_x lifetimes are small compared to NO_x resulting in localised increases only in the source areas at low latitudes. Above 25 km and in polar areas above ~ 10 km HO_x concentrations are reduced due to reaction with the additional NO_x ($OH + NO_2 \rightarrow HNO_3$). A reduced solar modulation potential ϕ (simulation PHI0) leads to an increase of ionization above the poles and additional production of HO_x. Here the reaction with the additional NO_x is not efficient enough to result in reduced HO_x concentrations in high latitudes. Instead, HO_x concentrations now decrease at low latitudes. Simulation M0PHI0 is a superposition of both effects and results in a net increase below ~ 20 km and a net decrease above 20 km.

4.1.3 Ozone concentrations

Figure 3 shows the response of ozone to the changes in NO_x and HO_x. In all four simulations with a weaker geomagnetic field (M10, M10P45, M10P0, M0) ozone concentrations show a significant decrease by more than 1 % above 20 km. The additional NO_x catalytically destroys ozone:

$$NO + O_3 \rightarrow NO_2 + O_2 \quad \text{(R1)}$$

$$NO_2 + O \rightarrow NO + O_2 \quad \text{(R2)}$$

$$O_3 + h\nu \rightarrow O_2 + O \quad \text{(R3)}$$

$$\text{Net}: 2O_3 \rightarrow 3O_2. \quad \text{(R4)}$$

HO_x, also able to destroy ozone catalytically, is enhanced in an area where ozone concentrations are predominantly determined by pure oxygen chemistry. Therefore the effect of the strongly increased HO_x concentrations in the tropical and subtropical UTLS on ozone remains marginal.

Ozone concentrations decrease significantly (−5 %) at the arctic tropopause. In addition to chemistry dynamics and feedback processes play an important role here. The additional NO_x in the Arctic leads to decrease in ozone in November. Consequently the polar stratosphere cools due to reduced absorption of outgoing infrared radiation. This enhances the pole to equator temperature gradient, leading to an intensification of the circumpolar vortex during its formation (more detailed discussion in dynamics section below, in particular Figs. 4 and 5). A stronger vortex in turn better insulates the arctic air masses, resulting in more radiative cooling and reduced ozone transport from the tropics, causing a positive feedback. The tropospheric ozone decrease is partly attributed to the reduced ozone transport from the lower stratosphere. After vortex breakup in spring, concentrations recover. Note that the feedback described above for M10P45 developed in response to only small differences in HO_x and NO_x compared to M10 and M0, which illustrates high sensitivity of atmospheric ozone chemistry and dynamics to minor differences in NO_x and HO_x.

In contrast to the Northern Hemisphere, it is interesting to see significant increases in ozone in the Southern polar UTLS (∼ 5 %). This is a robust feature in most simulations, in particular in M10P45. On the one hand, less ozone is destroyed due to less HO_x above 200 hPa. On the other hand, we argue for enhanced photochemical production of ozone. In contrast to the Northern Hemisphere, antarctic NO_x concentrations are naturally lower, because (i) colder temperatures cause higher denitrification in winter, and (ii) lightnings, a major natural NO_x source, are less common over the vast oceans than over land. The ozone chemistry over Antarctica is thus NO_x limited and additional NO_x can accelerate photochemical ozone formation. Support for this reasoning comes from comparison with the simulations M0PHI0 and PHI0, which show ozone increases in the southern hemispheric UTLS despite increases in HO_x. Furthermore do all three simulations first show augmented ozone concentrations at the edge of the Antarctic winter vortex and then successively towards the pole in austral spring (Fig. 5).

4.2 Changes in atmospheric dynamics

4.2.1 Zonal winds

Ozone and many other chemical species in the atmosphere absorb IR and UV radiation and thus influence temperature. Higher ozone concentrations in our simulations over Antarctica (Fig. 3), for example, lead to warming and a reduced pole to equator temperature gradient. This can cause a weakening of westerly winds with height due to the thermal wind relationship:

$$\boldsymbol{v}_\mathrm{T} = \frac{R}{f} \cdot \ln\left(\frac{p_0}{p_1}\right) \boldsymbol{k} \times \nabla_\mathrm{p} T. \quad (1)$$

where $\boldsymbol{v}_\mathrm{T}$ is the thermal wind vector, R is the specific gas constant for dry air, f is the Coriolis parameter, p_0 and p_1 are two pressure levels, $\boldsymbol{k}$ is the vertical unit vector and $\nabla_\mathrm{p} T$ is the temperature gradient on a constant pressure surface. We see significant anomalies in the mean annual zonal winds above ∼ 15 km altitude and at high

latitudes in the mean annual zonal wind fields for all our simulations. The general observations are easterly anomalies in the south and westerly anomalies in the north (Fig. 4). However, due to the semiannual reversal of stratospheric zonal wind direction and the high tropospheric variability mean annual wind anomalies are difficult to interpret and seasonal resolution is necessary to adequately analyse the wind changes and the processes involved.

Figure 5 illustrates the changes in ozone concentration and the zonal wind anomalies in January, August and November for M10P45. This simulation was exemplary chosen since it shows the strongest anomalies and conditions closely resemble the Laschamp Event. The Arctic vortex is significantly intensified in January due to low ozone concentrations and colder temperatures, while the lower-latitude westerlies become weaker. This is basically a slight shift of the tropospheric westerlies towards the pole. Note that similar observations and interpretations are made today in the Southern Hemisphere and are related to the man-made ozone hole and an altered temperature gradient in the UTLS. For comparison, temperatures in the lower stratosphere drop by 2 K in our simulation, while in today's ozone hole reductions of ~ 10 K can be observed. The detailed mechanisms how stratospheric ozone depletion can cause a shift of the tropospheric westerlies are still debated (Thompson and Solomon, 2002; Son et al., 2010; Polvani et al., 2011) and we will only briefly mention them here. We find mean annual sea level pressure anomalies of +0.5 hPa over Antarctica and −1 hPa over the Arctic compared to the reference simulation. This is a bias towards a high-index NH annular mode and a low-index SH annular mode. Annular modes are well studied patterns explaining large parts of climate variability in the Northern and Southern Hemisphere middle and high latitudes. Simultaneously, the tropopause is lowered over Antarctica (+2 hPa) and lifted over the Arctic (−3 hPa). A higher tropopause shifts the jet stream to higher latitudes and leads to an expansion of the Hadley cell, likely due to the interaction with baroclinic eddies (Son et al., 2010). We do, however, not fully understand why we do not see more pronounced antarctic wind anomalies in January, even though tropospheric ozone strongly increases and stratospheric ozone decreases. In August

a large positive ozone (and thus temperature) signal can be found between 40–70° S at 10–15 km altitude, slowly growing towards the pole in the following months. As a temperature maximum is found at $\sim 50^{\circ}$ at these altitudes in the winter hemisphere, the thermal wind relation predicts weaker stratospheric winds to the north and stronger winds to the south of the temperature anomaly in the Southern Hemisphere. With the positive ozone signal growing towards the pole during the austral winter and spring, also the negative wind pattern moves polewards. Finally in November the negative wind anomalies have moved 30° polewards and the SWW intensify on the equatorward edge. This is caused by the increase of antarctic ozone and warming of the polar air in spring. The equatorward shift of the SWW is most pronounced in austral spring and weakens again in summer. Note that the wind anomalies clearly reach into the troposphere, which cannot be explained by simple geostrophic wind theory. Instead the same argumentation as for today's downward control has to be used.

4.2.2 Seasonal surface winds and precipitation

Surface winds anomalies (shown in Fig. 6 for M10P45) allow us to examine spatial and seasonal variations in more detail. At high northern latitudes, a few westerly anomalies are statistically significant from December to May, which likely corresponds to the stratospheric intensification of the polar vortex described above. However, most of the surface wind changes in the Northern Hemisphere are not particularly systematic and only weak. This is also the case for the southern hemispheric surface winds from March to May. In JJA, however, the SWW significantly intensify on the polar edge and locally also in the core. IN SON, the SWW then shift significantly equatorward. This pattern persists for several months and is still faintly visible in DJF.

The simulations M10, M10P45, M10P0 and M0 all indicate slightly enhanced mean annual precipitation south of 40° S over Chile and Argentina, but these changes are not statistically significant on a 10 % significance level. M0PHI0 shows an insignificant decrease in precipitation and PHI0 virtually no change at all. Unfortunately, due to the low T31 resolution version of SOCOL-MPIOM, orographic precipitation in the Andes

cannot be fully captured. Given that the precipitation in the southern Andes is strongly controlled by the SWW (Garreaud, 2007), it may be more robust to tentatively interpret the above changes in the SWW as indirect proxy for precipitation and snow accumulation on the glaciers. The southward shift of the SWW in austral winter is in that regards probably most important, because austral winter is the crucial season for advecting moisture to the southern Central Andes between 30 and 40° S. For austral winter, our simulations thus basically show the opposite of the hypothesized northward shift during a geomagnetic event. It remains unclear at this point, whether the significant northward shift simulated for austral spring can compensate for that and whether the overall effect could be more positive glacier mass balances and glacier advances.

4.3 Paleoclimatic evidence for the Laschamp Event

As models per se may not include all relevant processes to perform adequate simulations, it is common practice to do model-data comparisons. We therefore attempted to review the most relevant paleoclimate records apart from the glacial chronologies that reach back to the Laschamp Event. This is challenging, because most records suffer from considerable dating uncertainties and the paleoclimatic interpretation of virtually all proxies is not straightforward. Note that controversies about the position and strength of the SWW during the last glacial maximum at ∼ 20 kyr go back already several decades, although many more paleodata and model studies have focused on that time period (Heusser, 1989; Markgraf et al., 1992; Kohfeld et al., 2013; Sime et al., 2013) than on the Laschamp Event. The few records from South America, which have been interpreted to record past changes in the SWW and related precipitation, do not provide a fully consistent picture. Low δ^{18}O values in the Laguna Tagua Tagua in Central Chile (34° S), for example, may reflect colder temperatures and/or enhanced winter precipitation from 40–20 kyr, while particularly arid conditions seem to have prevailed from 42.4–40.1 kyr (Valero-Garces et al., 2005). Pollen spectra in the Atacama desert further north (25° S) have been interpreted to document enhanced winter precipitation due to expanded southern westerlies from 40 to 33 kyr and from 24 to 14 kyr

(Maldonado et al., 2005). Stuut and Lamy (2004) on the other hand, argued for wet periods from 52 to 41 kyr and 40 to 38 kyr, but dry conditions from 38–28 kyr, based on grain-size analyses in a deep sea sediment core off the Chilean cost. Finally Hahn et al. (2013) reported increased biogenic silica contents between 41 and 37 kyr from the Laguna Potrok Aike in Argentina (52° S), yet the paleoenvironmental reasons for this increase remain unclear. This small compilation shows that at this point the available records don't help resolving the question whether the Laschamp Event may have affected the climate in the Southern Andes.

We also reviewed high-resolution, well dated records from outside the southern mid-latitudes. Speleothems in Brazil, for example, document increased precipitation at ∼ 39 kyr, whereas speleothems from China synchronously document more arid conditions (Wang et al., 2001, 2007). This anti-phasing in the speleothems, and many other published paleoclimate records, reflect a southward shift of the intertropical convergence zone at 39 kyr, which corresponds to Heinrich event 4 (Voelker, 2002; Hemming, 2004). Heinrich events are recurring episodes of massive ice-rafting in the North Atlantic during glacials, yet they are only the most severe of dozens of rapid and dramatic climate changes recorded in Greenland ice cores. Three of the so-called Dansgaard–Oeschger warming events occurred between 45 and 40 kyr (Greenland interstadials 9, 10 and 11) before the Heinrich event 4 started. There is no robust evidence for correlations between any of these events and geomagnetism (Nowaczyk et al., 2012). Vice versa, paleodata do not show a significant global climate impact of the Laschamp Event.

5 Conclusion and outlook

The results of our simulations indicate that geomagnetic events, as well as low solar modulation, have significant impacts on atmospheric chemistry and dynamics. We find substantial increases in hydrogen and nitrogen oxide concentrations as a consequence of enhanced ionization by GCRs. Ozone concentrations increase significantly (2–5 %)

at high southern latitudes and below ∼ 20 km in all our simulations, while concentrations decline at ∼ 30 km at all latitudes. Significant ozone destruction is observed at all altitudes over the Arctic in simulation M10P45, illustrating the sensitivity of the model to small initial differences in atmospheric chemistry and the importance of positive feedback mechanisms between atmospheric chemistry and dynamics.

Particularly the changing ozone concentrations are responsible for significant zonal wind anomalies, up to $5\,m\,s^{-1}$ in the stratosphere and $2\,m\,s^{-1}$ in the troposphere. The general response is a strengthening of the northern hemispheric vortex in boreal winter, and a weakening of the southern hemispheric vortex in austral winter and spring. Significant anomalies are also simulated for the surface winds, particularly an intensification of the SSW on their polar edge in austral winter and a pronounced northward shift during austral spring. It remains unclear at this point, whether related precipitation changes could have caused more positive glacier mass balances and glacier advances in the southern Central Andes during the Laschamp Event. Available paleodata from other records in southern South America are inconsistent. High-resolution polar ice core and subtropical speleothem records at least show that geomagnetic events very likely do not have direct and significant impacts on the global climate.

Future ensemble simulations would allow for more robust results and better statistics. Moreover, although our model does include an interactive ocean and sea ice component, 50 yr simulations might be too short to see possible oceanic feedbacks. Note also that this study investigated only the effects of GCRs on atmospheric ionization and the direct dynamical responses to changing atmospheric chemistry and temperature. Other mechanisms have been suggested, e.g. ionization-induced changes in nucleation and cloud formation, yet our understanding of these processes remains in its infancy (Kirkby, 2007). Last but not least, our model is able to simulate the effects of low and high energetic electrons from the sun and solar particle events (SPEs), and a follow-up study shall evaluate the possible effects of additional precipitating particles and such events during periods of weak geomagnetic fields.

Acknowledgements. We would like to thank Eugene Rozanov and Andrea Stenke for helpful comments at various stages of this research. Special thanks go to Markus Thürkow from FU Berlin for he kindly provided the initial land surface data set and ocean temperatures and we also express our greatest thanks for the ionization look-up table from Ilya Usoskin, originally developed for the work of Marco Calisto. J. Anet is supported by the Swiss National Science Foundation (SNF) under the grant CRSI122-130642(FUPSOL) and R. Zech acknowledges the support through SNF Ambizione PZ00P2_131670.

References

Anet, J. G., Muthers, S., Rozanov, E., Raible, C. C., Peter, T., Stenke, A., Shapiro, A. I., Beer, J., Steinhilber, F., Brönnimann, S., Arfeuille, F., Brugnara, Y., and Schmutz, W.: Forcing of stratospheric chemistry and dynamics during the Dalton Minimum, Atmos. Chem. Phys., 13, 10951–10967, doi:10.5194/acp-13-10951-2013, 2013. 6609

Bazilevskaya, G. A. and Svirzhevskaya, A. K.: On the stratospheric measurements of cosmic rays, Space Sci. Rev., 85, 431–521, doi:10.1023/a:1005029832052, 1998. 6611

Bazilevskaya, G. A., Usoskin, I. G., Flueckiger, E. O., Harrison, R. G., Desorgher, L., Buetikofer, R., Krainev, M. B., Makhmutov, V. S., Stozhkov, Y. I., Svirzhevskaya, A. K., Svirzhevsky, N. S., and Kovaltsov, G. A.: Cosmic ray induced ion production in the atmosphere, Space Sci. Rev., 137, 149–173, doi:10.1007/s11214-008-9339-y, 2008. 6607

Braconnot, P., Otto-Bliesner, B., Harrison, S., Joussaume, S., Peterchmitt, J.-Y., Abe-Ouchi, A., Crucifix, M., Driesschaert, E., Fichefet, Th., Hewitt, C. D., Kageyama, M., Kitoh, A., Laîné, A., Loutre, M.-F., Marti, O., Merkel, U., Ramstein, G., Valdes, P., Weber, S. L., Yu, Y., and Zhao, Y.: Results of PMIP2 coupled simulations of the Mid-Holocene and Last Glacial Maximum – Part 1: experiments and large-scale features, Clim. Past, 3, 261–277, doi:10.5194/cp-3-261-2007, 2007. 6610

Caballero-Lopez, R. A. and Moraal, H.: Limitations of the force field equation to describe cosmic ray modulation, J. Geophys. Res.-Space, 109, A01101, doi:10.1029/2003JA010098, 2004. 6609

Cai, W. and Cowan, T.: Trends in Southern Hemisphere circulation in IPCC AR4 models over 1950–99: ozone depletion versus greenhouse forcing, J. Climate, 20, 681–693, doi:10.1175/jcli4028.1, 2007. 6608

Calisto, M., Usoskin, I., Rozanov, E., and Peter, T.: Influence of Galactic Cosmic Rays on atmospheric composition and dynamics, Atmos. Chem. Phys., 11, 4547–4556, doi:10.5194/acp-11-4547-2011, 2011. 6607, 6609

Christl, M., Mangini, A., Holzkamper, S., and Spotl, C.: Evidence for a link between the flux of galactic cosmic rays and Earth's climate during the past 200 000 yr, J. Atmos. Sol.-Terr. Phys., 66, 313–322, doi:10.1016/j.jastp.2003.12.004, 2004. 6608

Denton, G. H., Heusser, C. J., Lowell, T. V., Moreno, P. I., Andersen, B. G., Heusser, L. E., Schluchter, C., and Marchant, D. R.: Interhemispheric linkage of paleoclimate during the last glaciation, Geogr. Ann. A, 81, 107–153, doi:10.1111/1468-0459.00055, 1999. 6607

Egorova, T. A., Rozanov, E. V., Zubov, V. A., and Karol, I. L.: Model for investigating ozone trends (MEZON), Izv. Atmos. Ocean. Phys., 39, 277–293, 2003. 6608

Egorova, T., Rozanov, E., Zubov, V., Manzini, E., Schmutz, W., and Peter, T.: Chemistry-climate model SOCOL: a validation of the present-day climatology, Atmos. Chem. Phys., 5, 1557–1576, doi:10.5194/acp-5-1557-2005, 2005. 6609

Espizua, L. E.: Pleistocene glaciations in the Mendoza Andes, Argentina, Quaternary Glaciations-Extent and Chronology, Pt 3: South America, Asia, Africa, Australia, Antarctica, edited by: Ehlers, J. and Gibbard, P. L., Elsevier, Amsterdam, the Netherlands, 2, 69–73, 2004. 6607

Garreaud, R. D.: Precipitation and circulation covariability in the extratropics, J. Climate, 20, 4789–4797, doi:10.1175/jcli4257.1, 2007. 6617

Gleeson, L. J. and Axford, W. I.: Solar modulation of galactic cosmic rays, Astrophys. J., 154, 1011–1026, doi:10.1086/149822, 1968. 6609

Hahn, A., Kliem, P., Ohlendorf, C., Zolitschka, B., Rosen, P., and Team, P. S.: Climate induced changes as registered in inorganic and organic sediment components from Laguna Potrok Aike (Argentina) during the past 51 ka, Quaternary Sci. Rev., 71, 154–166, doi:10.1016/j.quascirev.2012.09.015, 2013. 6618

Hemming, S. R.: Heinrich events: massive late pleistocene detritus layers of the North Atlantic and their global climate imprint, Rev. Geophys., 42, RG1005, doi:10.1029/2003rg000128, 2004. 6618

Heusser, C. J.: Southern Westerlies during the Last Glacial Maximum, Quaternary Res., 31, 423–425, doi:10.1016/0033-5894(89)90049-5, 1989. 6617

Hoyle, C.: Three dimensional chemical transport model study of ozone and related gases 1960–2000, Ph.D. thesis, ETHZ, Zürich, 2005. 6609

Jansen, E., Overpeck, J., Briffa, K., Duplessy, J.-C., Joos, F., Masson-Delmotte, V., Olago, D., Otto-Bliesner, B., Peltier, W., Rahmstorf, S., Ramesh, R., Raynaud, D., Rind, D., Solomina, O., Villalba, R., and Zhang, D.: Palaeoclimate, in: Climate Change 2007: The Physical Science Basis, Contribution of Working Group I to the Fourth Assessment Report of the Intergovernmental Panel on Climate Change, Report, Cambridge University Press, Cambridge, UK and New York, NY, USA, 2007. 6610

Kirkby, J.: Cosmic rays and climate, Surv. Geophys., 28, 333–375, doi:10.1007/s10712-008-9030-6, 2007. 6619

Kohfeld, K. E., Graham, R. M., de Boer, A. M., Sime, L. C., Wolff, E. W., Le Quere, C., and Bopp, L.: Southern Hemisphere westerly wind changes during the Last Glacial Maximum: paleo-data synthesis, Quaternary Sci. Rev., 68, 76–95, doi:10.1016/j.quascirev.2013.01.017, 2013. 6617

Liebowitz, A., Aydin, K. M., Verhulst, K. R., and Saltzman, E. S.: A comparison of Methyl Bromide measurements in ice core air from four Antarctic sites, AGU Fall Meeting Abstracts, Washington, D.C., USA, 2009. 6610

Lowell, T. V., Heusser, C. J., Andersen, B. G., Moreno, P. I., Hauser, A., Heusser, L. E., Schluchter, C., Marchant, D. R., and Denton, G. H.: Interhemispheric correlation of late pleistocene glacial events, Science, 269, 1541–1549, doi:10.1126/science.269.5230.1541, 1995. 6607

Maldonado, A., Betancourt, J. L., Latorre, C., and Villagran, C.: Pollen analyses from a 50 000 yr rodent midden series in the southern Atacama Desert (25 °30′ S), J. Quaternary Sci., 20, 493–507, doi:10.1002/jqs.936, 2005. 6618

Manzini, E., Giorgetta, M. A., Esch, M., Kornblueh, L., and Roeckner, E.: The influence of sea surface temperatures on the northern winter stratosphere: ensemble simulations with the MAECHAM5 model, J. Climate, 19, 3863–3881, doi:10.1175/jcli3826.1, 2006. 6608

Markgraf, V., Dodson, J. R., Kershaw, A. P., McGlone, M. S., and Nicholls, N.: Evolution of late Pleistocene and Holocene climates in the circum-South Pacific land areas, Clim. Dynam., 6, 193–211, 1992. 6617

Marsland, S. J., Haak, H., Jungclaus, J. H., Latif, M., and Roske, F.: The Max-Planck-Institute global ocean/sea ice model with orthogonal curvilinear coordinates, Ocean Model., 5, 91–127, doi:10.1016/s1463-5003(02)00015-x, 2003. 6609

Mix, A. C., Bard, E., and Schneider, R.: Environmental processes of the ice age: land, oceans, glaciers (EPILOG), Quaternary Sci. Rev., 20, 627–657, doi:10.1016/s0277-3791(00)00145-1, 2001. 6610

Nowaczyk, N. R., Arz, H. W., Frank, U., Kind, J., and Plessen, B.: Dynamics of the Laschamp geomagnetic excursion from Black Sea sediments, Earth Planet. Sc. Lett., 351, 54–69, doi:10.1016/j.epsl.2012.06.050, 2012. 6607, 6618

Polvani, L. M., Waugh, D. W., Correa, G. J. P., and Son, S.-W.: Stratospheric ozone depletion: the main driver of twentieth-century atmospheric circulation changes in the Southern Hemisphere, J. Climate, 24, 795–812, doi:10.1175/2010jcli3772.1, 2011. 6615

Porter, H. S., Jackman, C. H., and Green, A. E. S.: Efficiencies for production of atomic nitrogen and oxygen by relativistic proton impact in air, J. Chem. Phys., 65, 154–167, doi:10.1063/1.432812, 1976. 6609

Potgieter, M. S.: The modulation of galactic cosmic rays in the heliosphere: theory and models, Space Sci. Rev., 83, 147–158, doi:10.1023/a:1005014722123, 1998. 6607

Roeckner, E., Bäuml, G., Bonaventura, L., Brokopf, R., Esch, M., Giorgetta, M., Hagemann, S., Kirchner, I., Kornblueh, L., Manzini, E., Rhodin, A., Schlese, U., Schulzweida, U., and Tompkins, A.: The atmospheric general circulation model ECHAM 5, Part I: Model description, Report, Max-Planck-Institut für Meteorologie, Hamburg, Germany, 2003. 6608

Roeckner, E., Brokopf, R., Esch, M., Giorgetta, M., Hagemann, S., Kornblueh, L., Manzini, E., Schlese, U., and Schulzweida, U.: Sensitivity of simulated climate to horizontal and vertical resolution in the ECHAM5 atmosphere model, J. Climate, 19, 3771–3791, doi:10.1175/jcli3824.1, 2006. 6608

Rozanov, E. V., Zubov, V. A., Schlesinger, M. E., Yang, F. L., and Andronova, N. G.: The UIUC three-dimensional stratospheric chemical transport model: description and evaluation of the simulated source gases and ozone, J. Geophys. Res.-Atmos., 104, 11755–11781, doi:10.1029/1999jd900138, 1999. 6608

Rozanov, E. V., Schlesinger, M. E., and Zubov, V. A.: The University of Illinois, Urbana-Champaign three-dimensional stratosphere-troposphere general circulation model with interactive ozone photochemistry: fifteen-year control run climatology, J. Geophys. Res.-Atmos., 106, 27233–27254, doi:10.1029/2000jd000058, 2001. 6608

Saltzman, E. S., Aydin, M., Williams, M. B., Verhulst, K. R., and Gun, B.: Methyl chloride in a deep ice core from Siple Dome, Antarctica, Geophys. Res. Lett., 36, L03822, doi:10.1029/2008gl036266, 2009. 6610

Schilt, A., Baumgartner, M., Schwander, J., Buiron, D., Capron, E., Chappellaz, J., Loulergue, L., Schuepbach, S., Spahni, R., Fischer, H., and Stocker, T. F.: Atmospheric nitrous oxide during the last 140 000 years, Earth Planet. Sc. Lett., 300, 33–43, doi:10.1016/j.epsl.2010.09.027, 2010. 6610

Schraner, M., Rozanov, E., Schnadt Poberaj, C., Kenzelmann, P., Fischer, A. M., Zubov, V., Luo, B. P., Hoyle, C. R., Egorova, T., Fueglistaler, S., Brönnimann, S., Schmutz, W., and Peter, T.: Technical Note: Chemistry-climate model SOCOL: version 2.0 with improved transport and chemistry/microphysics schemes, Atmos. Chem. Phys., 8, 5957–5974, doi:10.5194/acp-8-5957-2008, 2008. 6609

Sime, L. C., Kohfeld, K. E., Le Quere, C., Wolff, E. W., de Boer, A. M., Graham, R. M., and Bopp, L.: Southern Hemisphere westerly wind changes during the Last Glacial Maximum: model-data comparison, Quaternary Sci. Rev., 64, 104–120, doi:10.1016/j.quascirev.2012.12.008, 2013. 6617

Sinnhuber, M., Nieder, H., and Wieters, N.: Energetic particle precipitation and the chemistry of the mesosphere/lower thermosphere, Surv. Geophys., 33, 1281–1334, doi:10.1007/s10712-012-9201-3, 2012. 6608

Solomon, S., Rusch, D. W., Gerard, J. C., Reid, G. C., and Crutzen, P. J.: The effect of particle precipitation events on the neutral and ion chemistry of the middle atmosphere: II. Odd hydrogen, Planet. Space Sci., 29, 885–892, doi:10.1016/0032-0633(81)90078-7, 1981. 6609

Son, S. W., Polvani, L. M., Waugh, D. W., Akiyoshi, H., Garcia, R., Kinnison, D., Pawson, S., Rozanov, E., Shepherd, T. G., and Shibata, K.: The impact of stratospheric ozone recovery on the Southern Hemisphere westerly jet, Science, 320, 1486–1489, doi:10.1126/science.1155939, 2008. 6608

Son, S. W., Gerber, E. P., Perlwitz, J., Polvani, L. M., Gillett, N. P., Seo, K. H., Eyring, V., Shepherd, T. G., Waugh, D., Akiyoshi, H., Austin, J., Baumgaertner, A., Bekki, S., Braesicke, P., Bruehl, C., Butchart, N., Chipperfield, M. P., Cugnet, D., Dameris, M., Dhomse, S., Frith, S., Garny, H., Garcia, R., Hardiman, S. C., Joeckel, P., Lamarque, J. F., Mancini, E., Marchand, M., Michou, M., Nakamura, T., Morgenstern, O., Pitari, G., Plummer, D. A., Pyle, J., Rozanov, E., Scinocca, J. F., Shibata, K., Smale, D., Teyssedre, H., Tian, W., and Yamashita, Y.: Impact of stratospheric ozone on Southern Hemisphere circulation change: a multimodel assessment, J. Geophys. Res.-Atmos., 115, D00M07, doi:10.1029/2010jd014271, 2010. 6615

Stenke, A., Schraner, M., Rozanov, E., Egorova, T., Luo, B., and Peter, T.: The SOCOL version 3.0 chemistry–climate model: description, evaluation, and implications from an advanced transport algorithm, Geosci. Model Dev., 6, 1407–1427, doi:10.5194/gmd-6-1407-2013, 2013. 6609

Stuut, J. B. W. and Lamy, F.: Climate variability at the southern boundaries of the Namib (Southwestern Africa) and Atacama (northern Chile) coastal deserts during the last 120 000 yr, Quaternary Res., 62, 301–309, doi:10.1016/j.yqres.2004.08.001, 2004. 6618

Thompson, D. W. J. and Solomon, S.: Interpretation of recent Southern Hemisphere climate change, Science, 296, 895–899, doi:10.1126/science.1069270, 2002. 6608, 6615

Toggweiler, J. R., Russell, J. L., and Carson, S. R.: Midlatitude westerlies, atmospheric CO_2, and climate change during the ice ages, Paleoceanography, 21, PA2005, doi:10.1029/2005pa001154, 2006. 6608

Usoskin, I. G. and Kovaltsov, G. A.: Cosmic ray induced ionization in the atmosphere: full modeling and practical applications, J. Geophys. Res.-Atmos., 111, D21206, doi:10.1029/2006jd007150, 2006. 6609

Usoskin, I. G., Alanko-Huotari, K., Kovaltsov, G. A., and Mursula, K.: Heliospheric modulation of cosmic rays: Monthly reconstruction for 1951–2004, J. Geophys. Res.-Space, 110, A12108, doi:10.1029/2005ja011250, 2005. 6609

Usoskin, I. G., Kovaltsov, G. A., and Mironova, I. A.: Cosmic ray induced ionization model CRAC : CRII: an extension to the upper atmosphere, J. Geophys. Res.-Atmos., 115, D10302, doi:10.1029/2009jd013142, 2010. 6609

Valcke, S.: The OASIS3 coupler: a European climate modelling community software, Geosci. Model Dev., 6, 373–388, doi:10.5194/gmd-6-373-2013, 2013. 6609

Valero-Garces, B. L., Jenny, E., Rondanelli, M., Delgado-Huertas, A., Burns, S. J., Veit, H., and Moreno, A.: Palaeohydrology of Laguna de Tagua Tagua (34°30′ S) and moisture fluctuations in Central Chile for the last 46 000 yr, J. Quaternary Sci., 20, 625–641, doi:10.1002/jqs.988, 2005. 6617

Valet, J.-P. and Valladas, H.: The Laschamp-Mono lake geomagnetic events and the extinction of Neanderthal: a causal link or a coincidence?, Quaternary Sci. Rev., 29, 3887–3893, doi:10.1016/j.quascirev.2010.09.010, 2010. 6608

Voelker, A. H. L.: Global distribution of centennial-scale records for Marine Isotope Stage (MIS) 3: a database, Quaternary Sci. Rev., 21, 1185–1212, doi:10.1016/s0277-3791(01)00139-1, 2002. 6618

Wang, X., Auler, A. S., Edwards, R. L., Cheng, H., Ito, E., Wang, Y., Kong, X., and Solheid, M.: Millennial-scale precipitation changes in southern Brazil over the past 90,000 years, Geophys. Res. Lett., 34, L23701, doi:10.1029/2007gl031149, 2007. 6618

Wang, Y. J., Cheng, H., Edwards, R. L., An, Z. S., Wu, J. Y., Shen, C. C., and Dorale, J. A.: A high-resolution absolute-dated Late Pleistocene monsoon record from Hulu Cave, China, Science, 294, 2345–2348, doi:10.1126/science.1064618, 2001. 6618

Zech, R., Kull, Ch., Kubik, P. W., and Veit, H.: LGM and Late Glacial glacier advances in the Cordillera Real and Cochabamba (Bolivia) deduced from ^{10}Be surface exposure dating, Clim. Past, 3, 623–635, doi:10.5194/cp-3-623-2007, 2007. 6607

Zech, R., May, J.-H., Kull, C., Ilgner, J., Kubik, P. W., and Veit, H.: Timing of the late Quaternary glaciation in the Andes from similar to 15 to 40° S, J. Quaternary Sci., 23, 635–647, doi:10.1002/jqs.1200, 2008. 6607

Zech, R., Zech, J., Kull, Ch., Kubik, P. W., and Veit, H.: Early last glacial maximum in the southern Central Andes reveals northward shift of the westerlies at 39 ka, Clim. Past, 7, 41–46, doi:10.5194/cp-7-41-2011, 2011. 6607

Table 1. Overview over the simulations that were carried out. The reference run has present day solar and geomagnetic fields. Dipole moment in % of 8.25×10^{22} A m^2. Phi in MV.

Run	Dipole moment	Latitude of pole	Phi
M10	10 %	78.5°	400
M10P45	10 %	45°	400
M10P0	10 %	0°	400
M0	0 %	78.5°	400
M0PHI0	0 %	78.5°	0
PHI0	100 %	78.5°	0
reference	100 %	78.5°	400

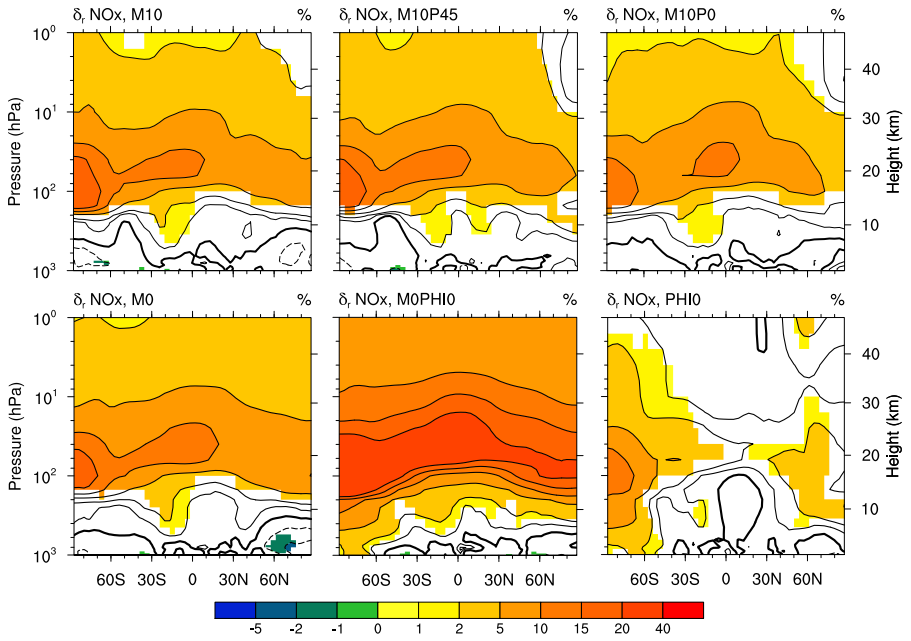

Fig. 1. Simulated effects on zonally averaged mean annual NO_x concentrations. The relative difference is defined as $([X]_{exp} - [X]_{ref})/[X]_{ref}$. Coloured areas are significant on a 5 % level. Solid contours indicate positive, dashed contours negative changes.

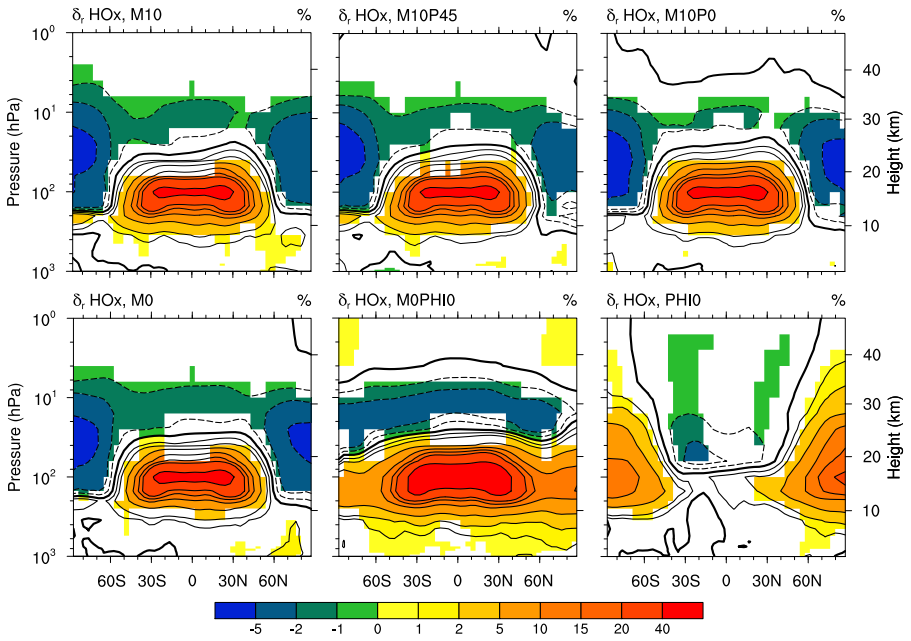

Fig. 2. Simulated effects on zonally averaged mean annual HO_x concentrations. Coloured areas are significant on a 5 % level. Solid contours indicate positive, dashed contours negative changes.

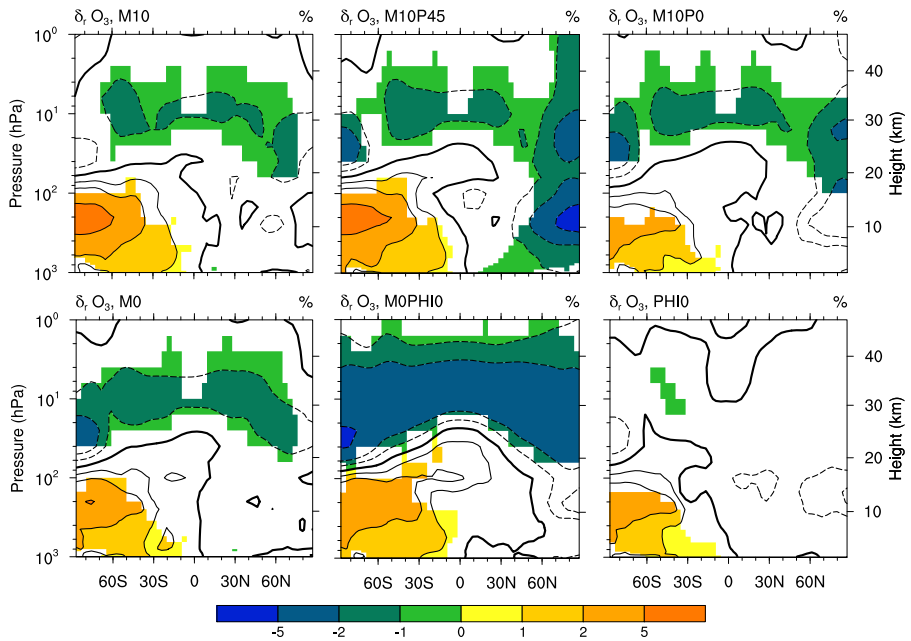

Fig. 3. Simulated effects on zonally averaged mean annual ozone concentrations. Coloured areas are significant on a 5 % level. Solid contours indicate positive, dashed contours negative changes.

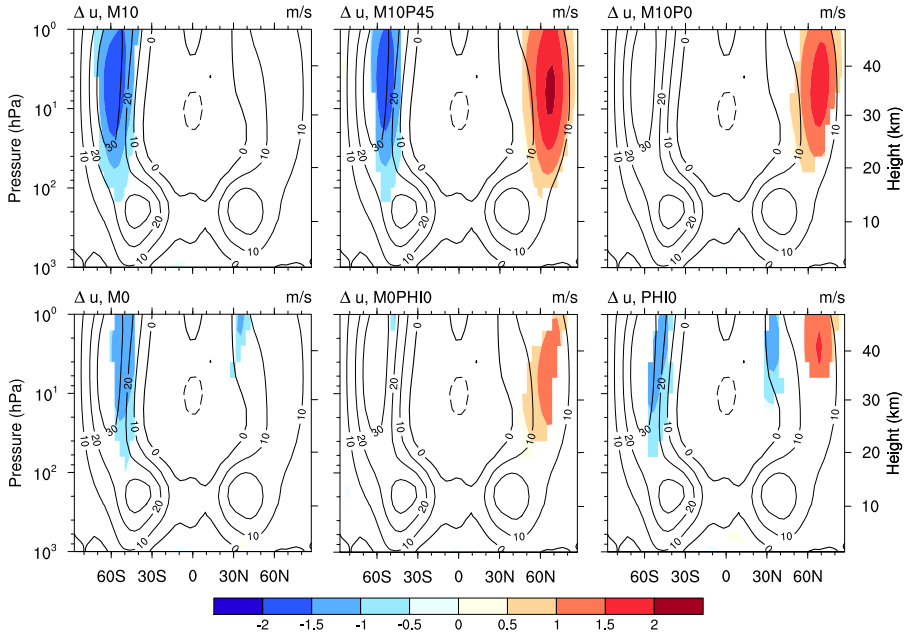

Fig. 4. Simulated effects on zonally averaged mean annual zonal wind (u). Coloured areas are significant on a 10 % level. Contours show the actual wind velocity of the reference run in 10 m s^{-1} intervals.

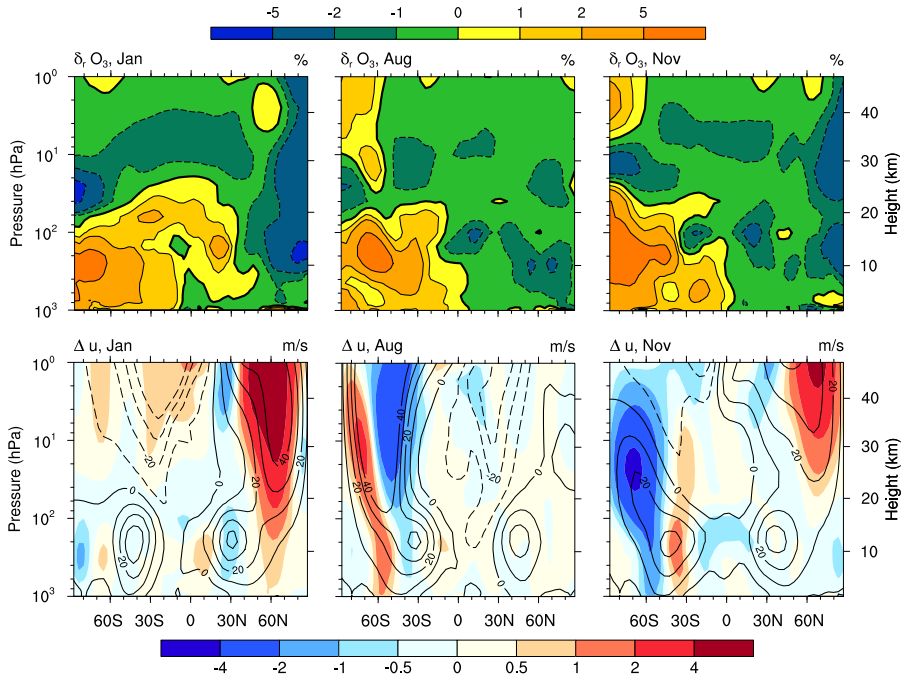

Fig. 5. Simulated monthly ozone anomalies (upper panel, as in Fig. 3) and zonal winds (lower panel, as in Fig. 4). Results are shown for simulation M10P45.

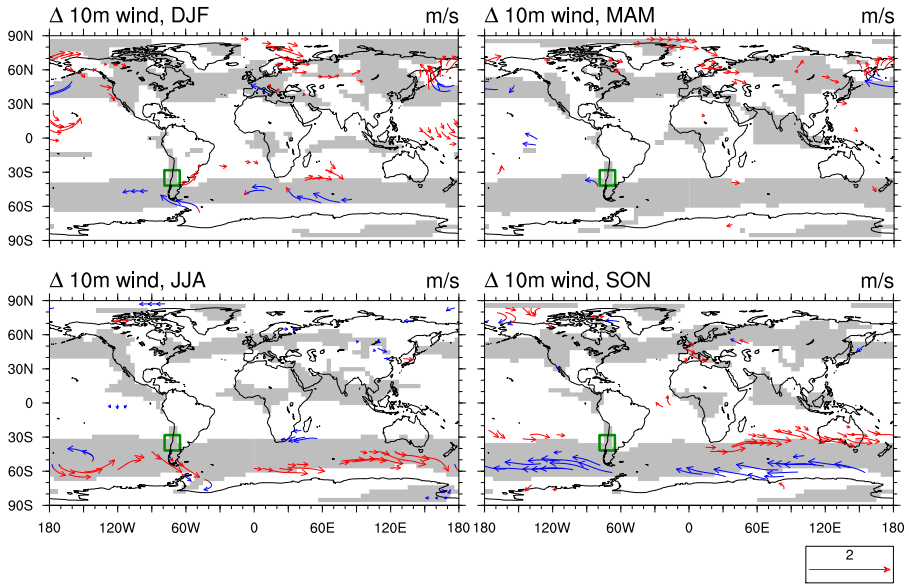

Fig. 6. Simulated effects on seasonal 10 m-surface winds. Results are shown for M10P45. Vectors show strength and direction of the change in 10 m wind. Vectors are colored based on the direction of change in zonal wind in the corresponding grid box (red for a significant increase, blue for a significant decrease in zonal component on a 10 % significance level). Only vectors with a significant change in wind, on a 10 % level, are shown. Grey contours show areas with positive zonal wind component (westerlies) of the reference run. The green square marks the southern Central Andes between 30 and 40°, where glacial maxima occurred at ~ 40 kyr.